Imaging of Bone Sarcomas and Soft-Tissue Sarcomas

Bildgebung von Knochen- und Weichteilsarkomen

Authors

Jasminka Igrec, Michael H. Fuchsjäger

Affiliation

Division of General Radiological Diagnostics, Department of Radiology, Medical University of Graz, Austria

Key words

bone sarcoma, soft tissue sarcoma, MR-imaging, ultrasound computed tomography (US/CT), radiomics, radiography

received 12.09.2020
accepted 09.02.2021
published online 26.03.2021

Bibliography

Fortschr Röntgenstr 2021; 193: 1171–1182
DOI 10.1055/a-1401-0215
ISSN 1438-9029

Georg Thieme Verlag KG, Rüdigerstraße 14, 70469 Stuttgart, Germany

Correspondence

Dr. Jasminka Igrec
Universitätsklinik für Radiologie, Klinische Abteilung für Allgemeine Radiologische Diagnostik, Medizinische Universität Graz, Auenbruggerplatz 9, 8010 Graz, Austria
Tel.: +43/3 16/38 58 04 34
jasminka.igrec@medunigraz.at

ZUSAMMENFASSUNG

Hintergrund Bei der Diagnose von Knochen- und Weichteilsarkomen hat die kontinuierliche Weiterentwicklung verschiedener bildgebender Verfahren die Erkennung kleiner Läsionen, die chirurgische Planung, die Beurteilung chemotherapeutischer Effekte und, was wichtig ist, die Anleitung für die Operation oder Biopsie verbessert.

Methode Diese Übersicht wurde auf der Grundlage einer PubMed-Literaturrecherche nach den Begriffen „Knochensarkom“, „Knochenkrebs“ und „Weichteilsarkom“, „Bildgebung“, „Magnetresonanztomografie“, „Computertomografie“, „Ultraschall“, „Radiografie“ und „Radiomics“ für den Publikationszeitraum 2005–2020 verfasst.

Ergebnisse und Schlussfolgerung Wie in dieser Übersicht diskutiert, spielen Radiografie, Ultraschall, CT und MRI eine Schlüsselrolle bei der bildgebenden Beurteilung von Knochen- und Weichteilsarkomen. In der täglichen Praxis ergänzen fortgeschrittene MRT-Techniken die Standard-MRT, werden aber nach wie vor zu wenig genutzt, da sie als zeitaufwändig, technisch anspruchsvoll und nicht zuverlässig genug angesehen werden, um Biopsie und Histologie zu ersetzen. PET/MRI und Radiomics haben sich als vielversprechend erwiesen, um in Zukunft zur Bildgebung von Sarkomen beizutragen.

Kernaussagen:

- Röntgenbilder sind bei diagnostischen Bildgebungsalgorithmen für Sarkome nach wie vor von entscheidender Bedeutung.
- US ist eine erste bildgebende Studie zur Beurteilung von oberflächlichen Weichteiltumoren.
- Die Rolle der CT entwickelt sich mit dem Entstehen neuer Techniken ständig weiter.
- Die MRT ermöglicht die nichtinvasive Beurteilung von Weichteil-, Knochen- und Gelenkstrukturen.
- Maschinelle Lernmethoden könnten die personalisierte Auswahl der Therapie für Patienten mit Sarkom verbessern.

ABSTRACT

Background In the diagnosis of bone and soft-tissue sarcomas, the continuous advancement of various imaging modalities has improved the detection of small lesions, surgical planning, assessment of chemotherapeutic effects, and, importantly, guidance for surgery or biopsy.

Method This review was composed based on a PubMed literature search for the terms “bone sarcoma,” “bone cancer” and “soft tissue sarcoma,” “imaging,” “magnetic resonance imaging”, “computed tomography”, “ultrasound”, “radiography”, and “radiomics” covering the publication period 2005–2020.

Results and Conclusion As discussed in this review, radiography, ultrasound, CT, and MRI all play key roles in the imaging evaluation of bone and soft-tissue sarcomas. In daily practice, advanced MRI techniques complement standard MRI but remain underused, as they are considered time-consuming, technically challenging, and not reliable enough to replace biopsy and histology. PET/MRI and radiomics have shown promise regarding the imaging of sarcomas in the future.

Key Points:

- Radiographs remain crucial in diagnostic imaging algorithms for sarcomas.
- US is an initial imaging study for the evaluation of superficial soft-tissue tumors.
- The role of CT continues to evolve as new techniques emerge.

- MRI allows the noninvasive evaluation of soft-tissue, osseous, and articular structures.
- Machine learning methods could improve personalized selection of therapy for patients with sarcoma.

Citation Format

- Igrec J, Fuchsjäger MH. Imaging of Bone and Soft-Tissue Sarcomas. Fortschr Röntgenstr 2021; 193: 1171–1182

Introduction

Bone and soft-tissue sarcomas represent a large, diverse group of mesenchymal-derived malignancies. According to the National Comprehensive Cancer Network (NCCN) guidelines, a multidisciplinary approach to the management of patients with primary bone and soft-tissue tumors is needed to achieve optimal results [1, 2].

In general, therapy is interdisciplinary and includes radiation therapy, systemic therapy, and surgery. Tumor response to systemic treatment correlates with the long-term prognosis, and its assessment is essential for planning future treatment.

Imaging, which is performed prior to any intervention, plays a crucial role in diagnosis, staging and restaging, monitoring response to treatment, and surveillance for recurrence. A radiological report is the cornerstone of the communication between radiology and the multidisciplinary team. Hence, it must be standardized, should describe the key findings that aid in planning further treatment, and should indicate the assumed etiology, providing a differential diagnosis in the case of equivocal findings. (▶ **Table 1**).

Due to the large variety of sarcoma subtypes, tumor features and treatment plans vary, and there is no single diagnostic pathway that determines the exact role of a particular imaging study (▶ **Table 2**).

Imaging techniques are rapidly evolving to address new and individualized treatment regimens [3–8] (▶ **Table 3**). In addition to conventional MRI (cMRI) sequences, advanced MRI techniques, including diffusion-weighted imaging (DWI), chemical shift imaging (CSI), dynamic contrast-enhanced MRI (DCE-MRI), MR spectroscopy (MRS), diffusion tensor imaging (DTI) are being assessed for sarcoma imaging.

However, these advanced imaging techniques are not ubiquitously accessible, and thus their exact roles have yet to be established.

This review focuses on using different imaging methods for the detection, characterization, local staging, and response assessment of primary bone and soft-tissue sarcomas.

Soft-tissue sarcomas

Soft-tissue sarcomas (STS) are uncommon tumors that account for roughly 1 % of solid cancers in adults, affecting all age groups. They represent a diverse group of neoplasms, including more than 80 different histological subtypes. This group displays a unique growth pattern, with a tendency to spread along fascial planes and within compartments in the line of least resistance [3, 9–11]. Approximately 60 % of STSs are localized in the extremities, 19 % appear in the trunk wall, 15 % in the retroperitoneum, and 9 % in the head and neck [12].

The main objectives of imaging are to detect and characterize a soft-tissue mass, to estimate its extent and its relation to adjacent structures within a muscle compartment, to determine the feasibility of resection, and to identify regional lymphadenopathy.

Ultrasound (US) is usually an initial imaging method used for the assessment of superficial soft-tissue tumors. It measures the dimensions and depth of the lesion, determines its relation to the fascia, its internal echotexture, and vascularity (color Doppler), and can differentiate a few typical benign tumors from pseudotumors (e. g., lipomas, ganglion cysts), and sometimes, hematomas and inflammatory collections from other equivocal lesions that need further evaluation. Contrast-enhanced US (CEUS) has recently been assessed for the diagnosis of soft-tissue tumors, especially for evaluating vascular tumor characteristics. Vital tumor tissue in malignancies shows earlier heterogeneous enhancement as compared to benign lesions with homogeneous or no enhancement [13]. The role of US elastography in STS is currently being validated [14].

Conventional radiography (CR), with at least two orthogonal views, is useful for detecting fat-containing lesions due to the displacement of the tissue planes, and for identifying vascular lesions or bone and soft tissue changes as part of inflammatory arthritis such as gout. CR can detect calcification, determine the calcification pattern, or depict the adjacent bone's pressure erosion [3, 11].

Given the advantages of MRI, concerning radiation exposure and contrast resolution, the applicability of computed tomography (CT) in the local assessment of STS is limited. However, CT has a role in evaluating calcified lesions (i. e., to rule out a myositis ossificans), identifying fat-containing lesions and differentiating calcification from ossification [3, 6]. When indicated, CT with contrast is a useful method for monitoring a local lesion, with comparable accuracy to MRI for the detection of recurrence greater than 15 cm^3 [15]. CT perfusion (pCT) imaging is a novel technique that provides both qualitative and quantitative imaging data regarding tumor microcirculation. Functional parameters obtained with pCT could be used as potential biomarkers for tumor response to various anticancer therapies targeting tumor vascularization [7].

MRI has become the cornerstone of musculoskeletal (MSK) radiology in the last decades due to its capacity to noninvasively assess soft-tissue, bone, and articular structures (▶ **Fig. 1**). The combination of cMRI and advanced MRI (aMRI) sequences enables state-of-the-art imaging of STS.

Delineating the tumor in relation to neurovascular structures, muscular compartments, and adjacent joints and determining the fascia-tumor relationship are essential for preoperative staging and planning of further treatment. MRI provides excellent characterization of tissues and enables adequate evaluation of local tumor extent, which is crucial for delineating safe surgical margins. Regarding the signal characteristics of lesions, Patel divides all soft-tissue masses into four categories (see ▶ **Table 4**) [6].

▶ **Table 1** The role of imaging methods in the evaluation of bone and soft-tissue tumors.

▶ **Tab. 1** Die Rolle der Bildgebung in der Behandlung von Knochen- und Weichteiltumoren.

ultrasound (US)	▪ detection and determination of the size and consistency of a superficial soft-tissue mass ▪ differentiation of solid mass from diffuse edema or from a cystic lesion ▪ detection of joint and tendon sheath effusion ▪ demonstration of relation between mass and adjacent neurovascular structures contrast-enhanced ultrasound (CEUS) – vascularity and perfusion of the lesion (viable tissue in malignant tumors shows early enhancement)
plain radiographs	▪ presence of intrinsic fat ▪ pattern of mineralization (myositis ossificans, tumoral calcinosis vs. sarcoma) ▪ calcification vs. ossification (cartilage vs. osteoid) ▪ detection of benign lesions: phleboliths – vascular lesions; amorphous mineralization and bone erosions in typical location – gout; osteocartilaginous masses – synovial chondromatosis ▪ character of interface between bone and soft tissue lesion (invasion or cortical remodeling) ▪ help in identifying bone lesions (e. g., osteochondroma)
computed tomography (CT)	▪ distinction between different types of tissue densities ▪ evaluation of mass mineralization where osseous anatomy is obscured or complex (spine, pelvis, soft tissue of the hand and feet) ▪ calcification vs. ossification (cartilage vs. osteoid) ▪ pattern of mineralization (myositis ossificans, tumoral calcinosis vs. sarcoma) ▪ character of interface between bone and soft-tissue lesion (invasion or cortical remodeling) ▪ staging ▪ local surveillance if MRI is contraindicated contrast-enhanced CT ▪ detection of isodense lesions on a non-contrast study ▪ cystic vs. solid lesion ▪ assessment of lesion vascularity and vascular invasion **CT- PERFUSION** ▪ evaluation of tumor angiogenesis ▪ monitoring therapy targeting tumor angiogenesis
magnetic resonance imaging (MRI)	▪ preoperative staging: – lesion size – relationship to neurovascular structures, fascial planes, muscle compartments, bone, and adjacent joints – vascular properties of the lesion ▪ biopsy planning ▪ postoperative monitoring ▪ monitoring of therapy response

▶ **Table 2** Checklist of the imaging findings in sarcoma reporting.

▶ **Tab. 2** Checkliste von Bildbefunden in der Sarkom-Berichterstellung.

tumor size	▪ transverse, vertical, and sagittal dimensions of the lesion ▪ distinctive shape of the lesion
location of the tumor	bone, muscle, or fascial plane involved
compartmental extent of the mass	distance of the lesion from the chosen anatomical landmark using a longitudinal plane of reconstruction (coronal or sagittal)
lesion characterization	intrinsic appearance of the lesion: ▪ high T1 W – fat or blood? ▪ nodularity, thickened septa ▪ high T2 W – homogeneity of the lesion – if heterogenous lesion – correlation with radiograph/CT (calcification/ossification) – suspicion for hemosiderin (additional gradient-echo image) ▪ contrast enhancement – pattern of enhancement (degree of necrosis; cystic vs. myxoid lesion; nodules or thick septations)
local invasiveness of the lesion	▪ STS: the extent of the peripheral reactive zone – "fascial tail" or a clear plane of separation ("split fat" sign) or pseudocapsule separating lesion from adjacent tissue ▪ BS: intra- and extraosseous soft tissue mass, bone marrow involvement, involvement of the growth plate and skip lesions within the same bone
invasion/ encasement of the vessels and nerves	relation to adjacent nerve and vascular structures
extension to the underlying bone or adjacent joint	relation to adjacent muscle, surrounding osseous structures, or joints
lymph node metastasis	regional lymph node involvement
distant metastasis	skip metastasis

For optimal therapy planning, further questions, especially regarding tumor location and extension, need to be addressed.

1. Healthy tissue surrounding STS is one of the crucial determinants of adequate resection margins. A wide excisional margin, defined as a distance of 2 cm from skin, fat, or muscle, and 1 mm from the fascia, is the primary surgical goal. For this reason, the differentiation of the reactive zone of edema from tumor infiltration of the fascia may be of great importance [11]. DCE-MRI and DWI are useful for evaluating tumor spread, especially for differentiating edema from tumor tissue [8]. Yoon et al. suggested adding DWI to cMRI, as it improves reader confidence in fascial involvement assessment [16].

▶ **Table 3** Value of MRI techniques in the diagnosis of bone and soft-tissue sarcomas.

▶ **Tab. 3** Der Wert von MRT-Techniken in der Diagnostik von Knochen- und Weichteilsarkomen.

T1-weighted imaging (T1WI)	▪ bone marrow evaluation ▪ characterization of anatomical relationship between lesion and surrounding structures ▪ characterization of lipomatous lesions
T2-weighted imaging (T2WI)	▪ tumor characterization – fluid-fluid levels ▪ evaluation of fascial planes
fat suppression (FS)	▪ detection of fat tissue in a lesion (hemangioma, lipoma) ▪ evaluation of the extent of edema ▪ increased conspicuousness of tumor vascularization in postcontrast T1WI
short tau inversion recovery (STIR)	▪ detection of changes with high T2 signal (tumor, inflammation, hemorrhage) (potential pitfall: overestimation of tumor extension)
susceptibility weighted imaging (SWI)/ gradient echo imaging (GE)	identification of increased susceptibility artifacts as evidence of prior hemorrhage (hemosiderin), metal, and air
gadolinium contrast enhancement (Gd-CE)	▪ identification of vessels and vascular involvement ▪ differentiation of solid hyperintense (myxomatous) or purely cystic lesions ▪ differentiation of solid, non-necrotic areas vs. fluid ▪ differentiation of edema from viable tumor ▪ delineation of hemorrhage (suspicion of underlying soft-tissue tumor) ▪ unequivocal findings **abstain from further imaging with Gd** if purely lipomatous tumor, anatomical asymmetry, and no tumor identified on the initial three scan sequences (T1w and T2w parallel to longitudinal tumor axis, T1w parallel to axial tumor axis)
subtraction	▪ elimination of misinterpretation of T1 shortening associated with hemorrhagic change as vascular enhancement ▪ in patients with metal fixation, no need for FS on postcontrast imaging
dynamic contrast-enhanced imaging (DCE-MRI)	▪ differentiation of necrosis ▪ differentiation of viable active tumoral tissue vs. nontumoral/necrotic areas – directing biopsy ▪ noninvasive assessment of response to radio- and chemotherapy ▪ information on tissue perfusion, vascularization, capillary permeability, volume of interstitial space ▪ differentiation of tumor vs. peritumoral edema ▪ monitoring treatment response: a) after starting neoadjuvant chemotherapy b) during surveillance after surgery
chemical shift imaging (CSI)	evaluation of bone marrow infiltration
diffusion-weighted imaging (DWI)	▪ qualitative and quantitative assessment of tissue cellularity and cell membrane integrity ▪ restriction of diffusion in malignant tumors – differentiation between benign and malignant tumors (pitfall: abscess, peripheral nerve sheath tumors) ▪ assessment of response to neoadjuvant therapy (residual vs. recurrent tumor vs. radiation-induced pseudotumor, postoperative granulation tissue, scarring) ▪ response to treatment
MR spectroscopy (MRS)	▪ largely a research tool ▪ elevation of the choline peak in malignant tumors – differentiation of benign from malignant lesions
diffusion tensor imaging (DTI)	reliable preoperative information about peripheral nerve involvement in STS

▶ **Table 4** Characterization of soft tissue lesions on magnetic resonance imaging.

▶ **Tab. 4** Charakterisierung von Weichteilläsionen in der Magnetresonanztomografie.

MRI signal characteristics	tissue type	diagnosis
1. intermediate T1WI high T2WI + postcontrast enhancement	myxoid	most sarcomas myxoma myxoid liposarcoma other myxoid sarcomas
2. high signal on T1WI high/intermediate T2WI	subacute blood proteinaceous fluid melanin	hemorrhagic tumors lymphangioma/ slow-flow vascular malformation melanoma/clear cell sarcoma
3. low T1WI and T2WI	fibrous hemosiderin calcification	highly cellular malignancies (e. g., lymphoma)
4. high T1WI (consistent with fat) fat suppression equal to fat (frequency-selective FS and short T1 inversion recovery)	lipomatous	liposarcoma (when conventional lipoma/ lipoma variants and hemangioma excluded): ▪ well-differentiated ▪ dedifferentiated ▪ pleomorphic – may not have any visible fat

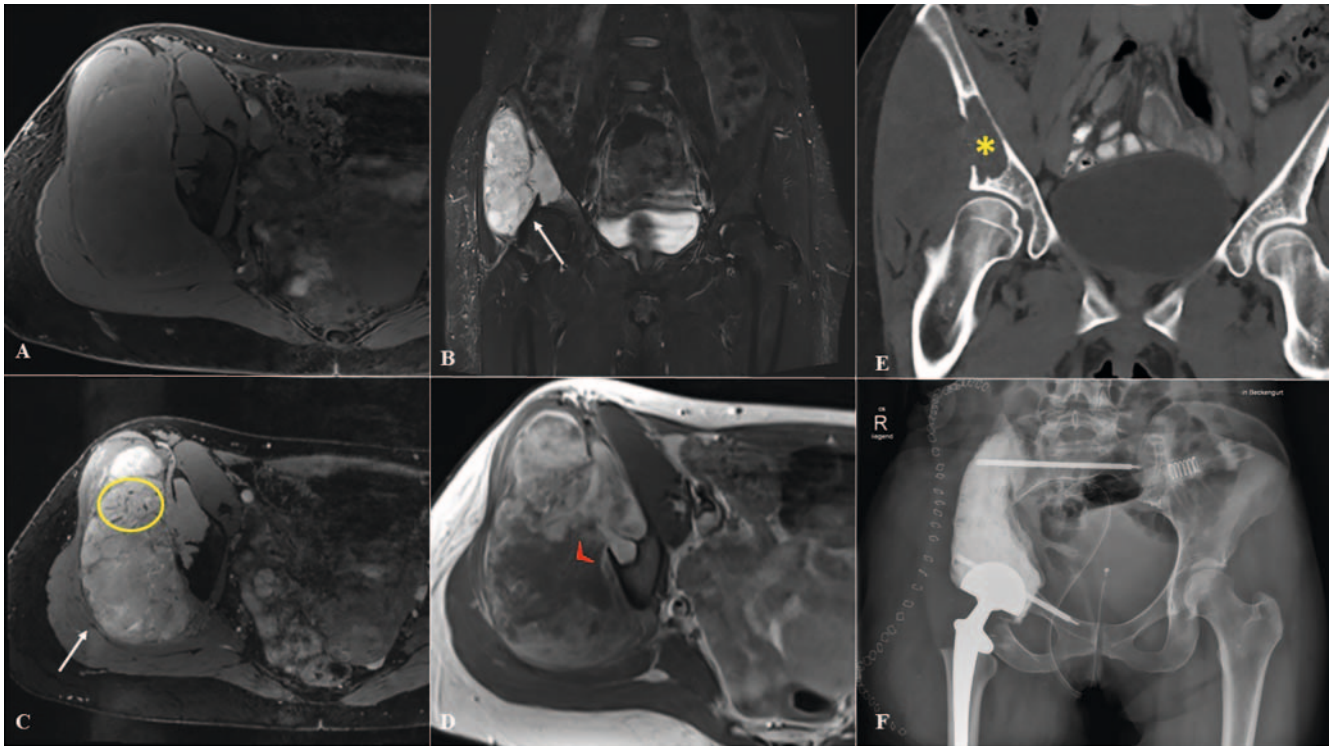

▶ **Fig. 1** A 35-year-old patient with spindle-cell sarcoma with EML-4-ALK fusion of the right iliac bone and gluteal region. **A** Soft-tissue tumor with osteodestruction of the underlying bone and a heterogeneous isointense signal is seen on the axial T1-weighted sequence. High signal and multilobulated appearance of the tumor due to septation with formed pseudocapsule (arrow) are seen on coronal **B** and axial **C** fat-saturated T2-weighted sequences. Small signal voids are seen within the lesion, presumably blood degradation products or vascular structures (ellipsoid). **D** After intravenous gadolinium application, heterogeneous enhancement of the lesion appears, with confluent hypovascular areas (arrowhead). **E** CT image of the pelvis in the coronal plane and bone window setting shows sharply demarcated osteolysis of the right iliac wing and acetabulum (asterisk). **F** Anteroposterior postoperative radiograph of the pelvis shows findings after right hemipelvectomy and proximal femur reconstruction, with the 3D-printed custom-made prosthesis of the right-sided pelvis and total endoprosthesis of the right hip joint.

▶ **Abb. 1** MRT eines 35-jährigen Patienten mit Spindelzellsarkom und EML-4-ALK Fusion des Os ilium und der Glutealregion rechts. **A** Weichteiltumor mit Osteodestruktion des angrenzenden Knochens und heterogen-isointensem Signal in der axialen T1-gewichteten Sequenz. In der koronalen **B** und axialen **C** fettgesättigten T2 gewichteten Sequenz erscheint der Tumor hyperintens sowie multilobuliert aufgrund von Septierungen und Pseudokapsel-Formierungen. Innerhalb der Läsion zeigen sich kleine Flow-Voids, mutmaßlich Blutabbauprodukten oder vaskulären Strukturen entsprechend (Ellipse). **D** Nach intravenöser Gadolinium Applikation weist die Läsion ein heterogenes Enhancement mit konfluierenden hypovaskulären Arealen (Pfeilspitze) auf. **E** In der CT des Beckens in axialer Schichtung zeigt sich im Knochenfenster-Kernel eine scharf begrenzte Osteolyse der rechten Beckenschaufel und des Acetabulums (Stern). **F** Postoperatives AP Beckenröntgen nach Hemipelvektomie rechts und proximaler Femurrekonstruktion mittels einer 3D-gedruckten, individuell angefertigten Prothese des rechten Beckens und einer Totalendoprothese des rechten Hüftgelenkes.

2. Additionally, cMRI has its limits with respect to distinguishing residual tumor from reactive changes after neoadjuvant therapy, as both residual tumor and posttreatment scar tissue enhance after injection of contrast. DCE-MRI overcomes this problem in the pre- or posttreatment setting by providing information about the tissue's vascular properties by discriminating different contrast enhancement patterns. Utilizing a gradient-echo (GE) sequence after dynamic Gd injection enables differentiation of rapid enhancement of viable tumor tissue from non-enhancing necrosis, late-enhancing posttherapy changes, peritumoral edema, or granulation tissue [8, 17].

3. In STS, tumor size, location, depth, and the French Federation of Cancer Centers Sarcoma Group (FNCLCC) histologic grading system (based on tumor differentiation, tumor necrosis, and mitotic activity) are the most important prognostic factors [18]. Differentiation between low- and high-grade STS is critical in treatment decision-making (in comparison to patients with low-grade STS, patients with high-grade STS have a worse outcome, develop metastases more frequently, and/or have a greater incidence of recurrent disease). Unfortunately, due to tumor heterogeneity, the preliminary tumor grading derived on biopsy specimens may differ from the final grade provided on the surgical specimen, leading to prognostic uncertainty and treatment delay [19, 20]. Recent studies suggest that aMRI can overcome this problem and MRI findings are concordant with prognostic information obtained from the histologic grade [11, 21, 22]. Furthermore, these MRI techniques have higher specificity in depicting tissue heterogeneity, which helps in guiding the biopsy [8]. Studies by Crombe et al. and Bologna et al. showed that features derived from cMRI (such as tumor heterogeneity, amount of necro-

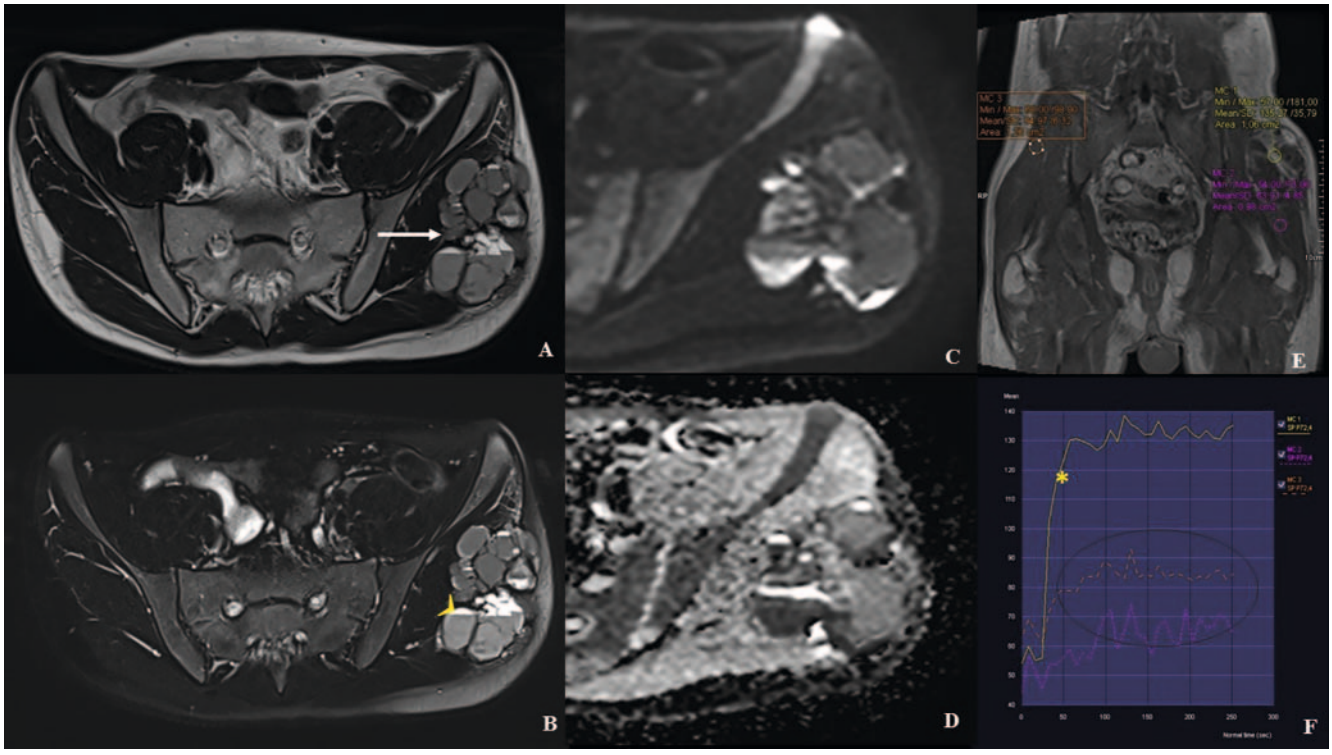

▶ **Fig. 2** A 16-year-old male patient with angiomatoid fibrous histiocytoma of the left gluteal region. **A** Axial T1-weighted image shows multilobulated cystic-solid mass between gluteus maximus and medius with fluid-fluid levels (white arrow). **B** Focal areas of T2 signal presumably represent areas of blood of variable age (yellow arrowhead). Diffusion restriction of the solid parts of the tumor on DWI and ADC map **C**, **D**. **E**, **F** The areas of intense enhancement correlate with a type III TIC (rapid early enhancement followed by plateau with limited specificity for tumor characterization, suspicious for malignancy) (yellow star). Black ellipsoid = reference standard of arterial uptake.

▶ **Abb. 2** MRT eines 16-jährigen Patienten mit angiomatoidem fibrösem Histiozytom der linken Glutealregion. **A** In der axialen T1w zeigt sich eine multilobulierte zystisch-solide Raumforderung zwischen Gluteus maximus und medius mit Flüssigkeitsspiegeln (weißer Pfeil). **B** Fokale T2w-Signalsteigerungen, mutmaßlich Blutprodukten unterschiedlichen Alters entsprechend (gelbe Pfeilspitze). **C**, **D** Diffusionsrestriktion der soliden Tumoranteile in der DWI und ADC. **E**, **F** Die Areale mit kräftigem Enhancement korrelieren mit einem Typ III TIC (schnelles und frühes Enhancement, gefolgt von einer Plateauphase mit eingeschränkter Spezifität für die Tumorcharakterisierung; Malignitätssuspekt) (gelber Stern). Schwarze Ellipse = Referenzstandard für arterielle Kontrastmittelanreicherung.

sis, and peritumoral enhancement) are independent predictors of tumor grade and are associated with high-grade tumors [4, 22] (▶ **Fig. 2**). A recent study by Lee et al. highlighted the added value of DWI in sarcoma imaging. By correlating DWI and DCE-MRI parameters with the Ki-67 labeling index (LI), the authors showed that the mean ADC value was significantly and inversely correlated with the Ki-67 LI ($\rho = -0.333$, $p = 0.047$). In contrast to the high-proliferation group of STS, the low-proliferation group showed a significantly higher mean ADC value when a cut-off of $1.16 \times 10^{-3} mm^2/s$ was used, with a sensitivity, specificity, and area under the curve for differentiating low- and high-proliferation groups of 75.0 %, 60.0 %, and 0.712, respectively ($p = 0.014$). DCE-MRI parameters in the study did not show a statistically significant correlation with Ki-67 LI [23].

A relatively novel method in MSK radiology, i. e., MRS, yields information regarding the lesion's metabolism by measuring metabolites that are abundantly produced by malignant tumors, particularly choline (Cho)-containing compounds, enabling better tissue characterization and treatment response evaluation. Consequently, this method can differentiate benign from malignant soft-tissue tumors in pre-surgical and posttreatment settings [24]. Patel et al. showed that a discrete elevated Cho-peak could diagnose malignancy with a sensitivity and specificity of 88 % and 68 %, respectively. In comparison, a low concentration (< 0.3 mmol/kg) has a negative predictive value of 100 % for excluding malignancy [6]. In our opinion, the limitation and the most probable reason this method has not yet been implemented in standard practice is that it is technically challenging and has potential pitfalls. Specifically, an elevated Cho-peak can also be perceived in metabolically active benign lesions, such as peripheral nerve sheath tumors. Furthermore, as a marker of tissue damage, a lipid peak is observed in various conditions, including tumors after oncological treatment as well as inflammatory collections [8].

Bone sarcomas

Primary bone tumors account for less than 0.2 % of all cancers. They frequently affect the young population, in whom they exhibit an aggressive growth pattern and high mortality and disability rates. In general, osteosarcoma (OS) is the most common primary

malignant bone tumor, excluding malignancies of marrow origin, followed by chondrosarcoma (CS) and Ewing sarcoma (ES). The latter represents the second most common primary malignant bone tumor in children and adolescents. Compared to OS and ES, which mostly affect children and young adults, CS usually occurs in adult patients, most commonly in the fourth and fifth decade of life [1, 25–27] (▶ **Fig. 3**).

The main objectives of imaging are to determine the size and the intramedullary extension of the lesion and the infiltration of the growth plate, muscle compartments, surrounding neurovascular structures, and joints, to detect skip lesions, to plan the optimal biopsy site, to establish the type of surgical resection, and to evaluate regional lymph node involvement.

An appropriate selection of various imaging techniques in the diagnostic workup of a patient with suspected primary bone sarcoma (BS) is essential for successful diagnosis and treatment [28]. An osteolytic or osteoblastic bone lesion, >aggressive periosteal reaction, tumor matrix, and heterogeneous post-contrast enhancement are the key imaging features of malignant bone tumors. Nowadays, there are numerous noninvasive, technologically advanced imaging methods for evaluating BS, including CT, MRI, and nuclear imaging. However, radiographs of the entire bone in two orthogonal projections, together with the adjacent joint, remain essential for detecting skeletal lesions and should be obtained early in the diagnostic process in any symptomatic patient. For most osseous lesions, an appropriate differential diagnosis can be provided using the patient's age, lesion location, and radiographic appearance [25–27, 29]. On CR, the bone destruction pattern (geographic vs. non-geographic), a zone of transition, cortical destruction, type of periosteal reaction, and soft-tissue and joint involvement are determined. These features help differentiate indolent from aggressive bone tumors [30] (▶ **Fig. 4**).

While the role of CT in the local staging of BS has declined, it remains the standard method for evaluating uncertain radiographic and scintigraphy findings of the spine and pelvis. Due to its high sensitivity in detecting calcifications and ossifications, CT is preferable to CR for determining the tumor matrix and depicting occult matrix mineralization. Additionally, it allows better estimation of the depth and degree of endosteal scalloping [25, 26]. Infiltration of the growth plate and intra-articular extension can occur depending on the type of sarcoma and tumor growth rate. Although CT enables the detection of the changes surrounding the growth plate, it does not allow evaluation of physeal invasion as reliably as MRI (PPV, NPV, and accuracy were 81.5 %, 100 %, and 86.5 %, respectively, with CT in comparison to 87.1 %, 100 %, and 90.3 %, respectively, with MRI) [31].

In the diagnostic algorithm, MRI is the superior modality for detecting bone marrow infiltration and determining tumor extent, in agreement with the UICC/AJCC staging system [28, 32]. Although MRI has excellent specificity for classifying different subtypes of periosteal reaction [30], the lesion's true nature and aggressiveness are much more accurately determined with CR. Consequently, MR images should always be assessed in combination with recent radiographs [33]. The MRI protocol has to include the entire tumor with the whole anatomical compartment and adjacent joints, as skip lesions greatly influence treatment planning [34]. An unenhanced T1-weighted MRI (T1 W) examination is essential to accurately determine the extent of a tumor before surgery. A study by Gulia et al. compared BS (OS, ES, and CS) measurements on MRI with the histopathological extent seen on resected specimens. For all BS types, the authors demonstrated a strong correlation between tumor size determined histopathologically after resection and the tumor size estimated by MRI preoperatively [35].

According to the American College of Radiology (ACR) Appropriateness Criteria for Bone Tumors, sufficiently high contrast between the tumor and healthy marrow on non-enhanced images enables optional intravenous (IV) administration of Gd in the evaluation of primary bone tumors [28]. With the help of CSI, a novel fast imaging technique, a marrow-replacing tumor can be identified and distinguished from a benign infiltrative process such as a bone marrow edema or hematopoietic marrow [36] (▶ **Fig. 5**). Nevertheless, Gd application will better identify solid tumor areas, areas of necrosis, hemorrhage (necessary for biopsy planning), and joint involvement [3, 8, 37]. If not contraindicated, in our institution, we routinely perform additional postcontrast T1 W sequences on two planes.

As stated above, cMRI is currently the best imaging method for detecting and characterizing MSK tumors, but it cannot provide crucial information regarding tumor cellularity. In BS, an advanced sequence like DWI can evaluate tumor cellularity, primarily via quantifiable parameters like mean ADC, and therefore differentiate necrosis from viable tumor tissue, i. e., during response evaluation [5, 38]. Caution should be used when evaluating myxomatous, cystic, and cartilaginous components of primary BS, in which ADC values are significantly higher than those of other malignant bone tumors (▶ **Fig. 6**). Regarding the sensitivity and specificity of DWI and ADC when differentiating benign from malignant primary BS, Rao et al. showed that CS had the highest ADC values, reaching as high as 2.99×10^{-3} mm2/s, while ES had the lowest ADC values, reaching as low as 0.56×10^{-3} mm2/s. The authors suggested that higher ADC value in CS might be due to cellularity variations within a cartilaginous stroma [38]. Not only in STS but also in BS, DWI can estimate the residual tumor tissue's vitality after treatment and detect recurrence at an early stage when curative treatment is still possible [8].

MRS with metabolite quantification helps characterize primary bone lesions. In the literature, the sensitivity and specificity of MRS for detecting the Cho-compound in BS and STS are around 70 % and 75 %, respectively [39]. Malek et al. compared the DWI and multivoxel proton MRS findings in OS with those in normal muscle on a 3-Tesla MR system. The authors demonstrated that visual confirmation of diffusion restriction is sufficient for detecting tumoral tissue without further need for quantification of ADC values. Furthermore, MRS showed a statistically higher maximum Cho/Cr-ratio of OS than of normal muscle, 1.94 ± 1.12 vs. 1.34 ± 0.11, respectively [40].

As in STS, DCE-MRI in BS is used for tissue characterization, identifying areas of proliferating tumor tissue needed for biopsy, and monitoring response to neoadjuvant chemotherapy [41]. It shows encouraging results in post-therapeutic follow-up, distinguishing tumor from reactive edema after chemotherapy and residual tumor from postoperative granulation tissue [36]. Furthermore, in

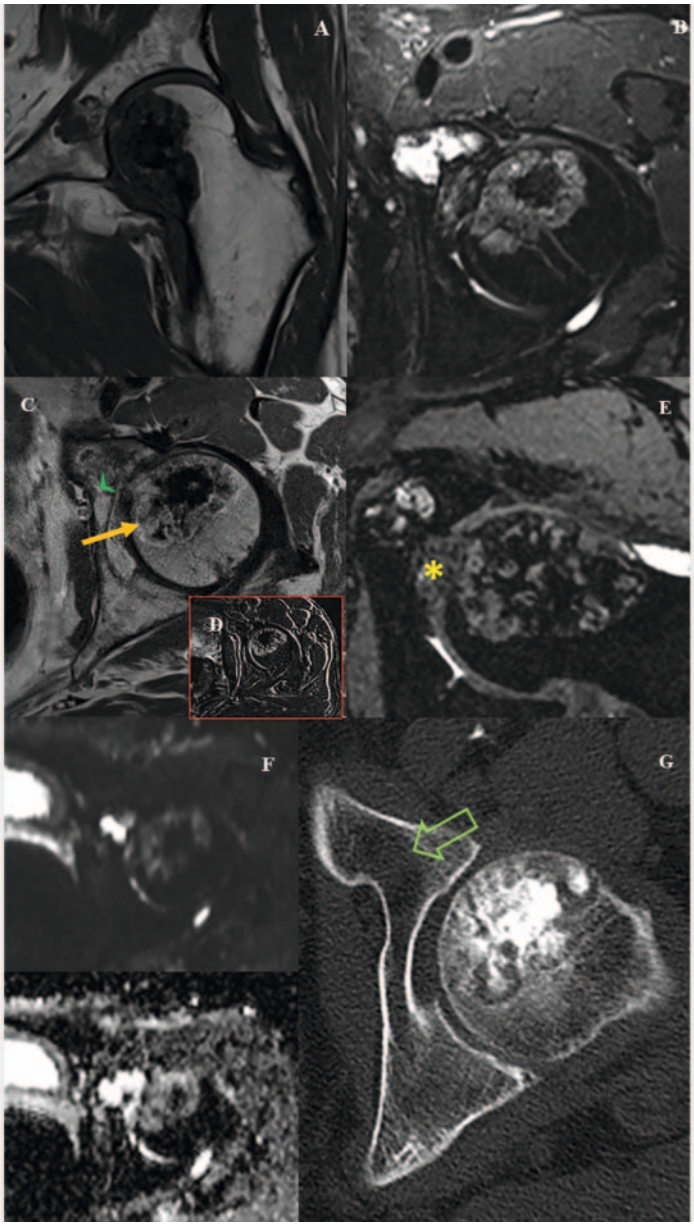

▶ **Fig. 3** A 58-year-old male patient with high-grade chondrosarcoma of the femoral head and clear-cell chondrosarcoma of the acetabulum. Coronal T1-weighted sequence **A** shows an intermediate signal of the tumor in the femoral head with central low-signal areas corresponding to matrix calcification. The lesion in the acetabulum shows an intermediate to low signal. **B** Very high signal intensity is seen in non-mineralized portions of the tumors in axial fat-saturated T2-weighted sequence corresponding to cartilaginous matrix. **C** T1-weighted sequence after gadolinium application and additional subtraction image **D** show peripheral rim-like enhancement of the lesion in the femoral head (yellow arrow) and moderate heterogeneous contrast enhancement of the lesion in the acetabulum (green arrowhead). **E** DESS (Double Echo Steady State) sequence shows infiltration of the articular cartilage and the intraarticular extension of the femoral tumor (yellow star). **F** The lesions show no restricted diffusion on DWI- and ADC-map. **G** Corresponding axial CT, in bone window, the lesion in the femoral head shows cortical remodeling and extension to the cortex with permeative appearance. The pure osteolytic lesion in the acetabulum is seen with an intact cortex (hollow green arrow).

▶ **Abb. 3** 58-jähriger Patient mit high-grade Chondrosarkom des Femurkopfes und klarzelligem Chondrosarkom des Acetabulums. **A** Intermediäre Signalintensitäten des Tumors im Femurkopf in der coronalen T1w mit zentral hypointensen Arealen, welche Matrix-Kalzifizierungen entsprechen. Die Läsion im Acetabulum weist ein intermediäres bis hypointenses Signal auf. **B** Hohe Signalintensitäten sind in den nicht-mineralisierten Anteilen des Tumors in der axialen fettgesättigten T2w sichtbar, korrespondierend zu kartilaginärer Matrix. **C** In der T1w nach Gadolinium-Applikation und dem zusätzlichen Subtraktionsbild **D** zeigt sich ein peripheres Randenhancement der Läsion im Femurkopf (gelber Pfeil), sowie ein moderates heterogenes Enhancement der Läsion im Acetabulum (grüner Pfeil). **E** In der DESS (Double Echo Steady State) Sequenz sind eine Infiltration des Gelenksknorpels und eine intraartikuläre Ausdehnung des femoralen Tumors (gelber Stern) abgrenzbar. **F** In der DWI und ADC weisen beide Läsionen keine Diffusionseinschränkung auf. **G** Die korrespondierende axiale CT im Knochenfenster-Kernel zeigt ein kortikales Remodeling, eine Extension bis an die Kortikalis und eine permeative Erscheinung der Läsion im Femurkopf. Die an die ausschließlich osteolytische Läsion des Acetabulums angrenzenden Kortikalisanteile erscheinen intakt (hohler grüner Pfeil).

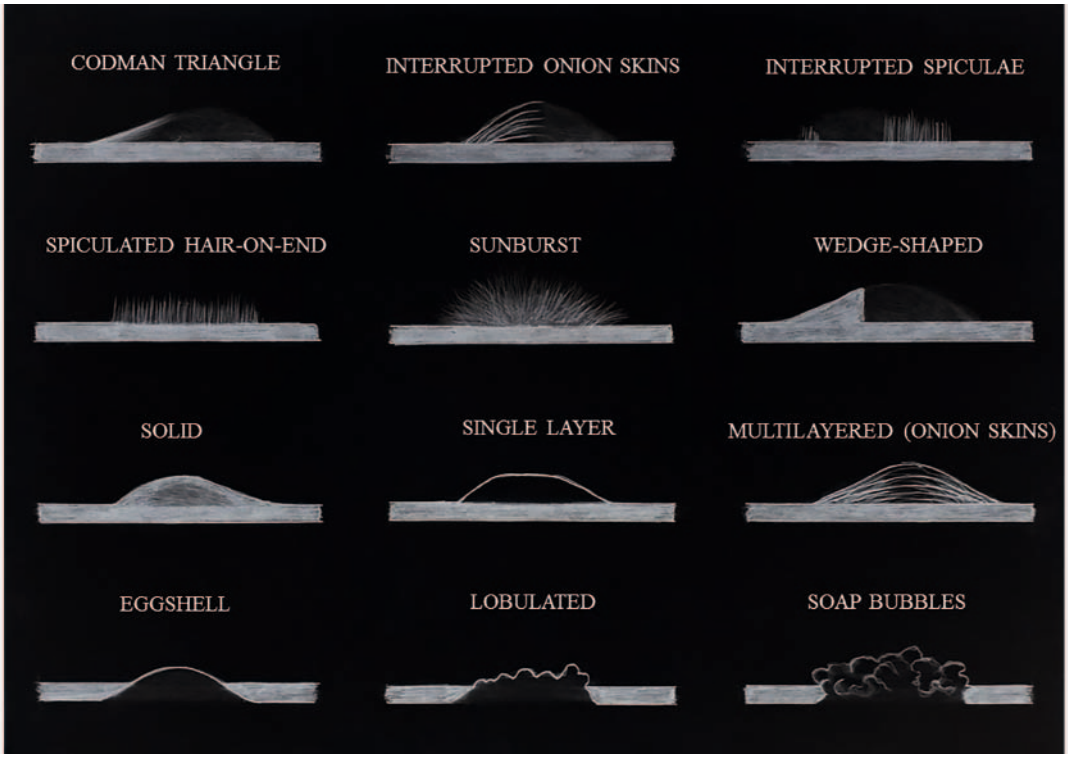

▶ **Fig. 4** Patterns of periosteal reaction. Continuous periosteal reaction: eggshell, lobulated, soap bubbles, solid, single layer, multilayered (onion skins), spiculated (hair on end), sunburst; interrupted periosteal reaction: wedge-shaped, Codman triangle, interrupted onion skins, interrupted spiculae. Image courtesy of Renato Igrec, MD.

▶ **Abb. 4** Muster der Periostreaktion. Kontinuierliche Periostreaktion: Eierschalen-artig, lobuliert, Seifenblasen-artig, solide, einschichtig, mehrschichtig (Zwiebelschalen-artig), spikuliert („hair-on-end“ „Bürstensaum“-Phänomen), divergierende Spiculae („Sun-burst“-Phänomen); unterbrochene Periostreaktion: Strebepfeiler-Form, Codman-Dreieck, unterbrochene Zwiebelschalen, unterbrochene Spiculae. Bilder mit freundlicher Genehmigung von Dr. Renato Igrec.

BS, DCE-MRI and DWI permit recognition of chemotherapy-induced tumor necrosis. In OS and ES, as a result of chemotherapy treatment, neo-angiogenesis decreases, subsequently causing necrosis, resulting in reduced tumor size with better tumor delineation from surrounding tissues [35, 37].

For patients with an absolute contraindication to MRI examination, dual-energy CT (DE-CT) may have a potential role in bone marrow imaging. It helps differentiate bone marrow edema from soft tissue infiltration, provides additional information regarding tissue composition, reduces metal artifacts, and optimizes image quality [42, 43].

Future outlook

Nowadays, attention is focused on developing hybrid systems that could enable a complete diagnostic evaluation for BS and STS in one session with the lowest possible radiation risk (significant in pediatric patients) [44]. Integrated PET/MRI is an evolving imaging modality, which combines the excellent soft-tissue contrast resolution of MRI with the functional metabolic capabilities of PET. This method has yielded encouraging results with respect to improving staging, preoperative and radiation therapy planning, and the evaluation of treatment response while decreasing cumulative radiation dose in children as well as in adult patients with sarcoma [45, 46]. Further studies are needed to establish its definitive future role.

The introduction of artificial intelligence (AI) in MSK radiology and the employment of radiomic texture analysis have resulted in the development of radiomic MRI-based models that could help distinguish low-grade from high-grade sarcomas [47, 48]. In a study by Malinauskaite et al., radiomics incorporated with machine-learning methods performed better than specialized MSK radiologists, reaching a diagnostic accuracy of 94.7 % [49]. Additionally, radiomic features extracted from MRI show promise as biomarkers for predicting overall survival in patients with STS. In the future, combining models using clinical and radiomic features could optimize treatment and enable personalized management of patients with sarcoma [50].

Conclusion

The incorporation of various imaging modalities in the diagnostic algorithm for mesenchymal tumors has contributed to the improvement of the diagnosis, surgical planning, and assessment of oncological therapy effectiveness. The role of MRI in the evaluation of MSK tumors continues to evolve while new hybrid tech-

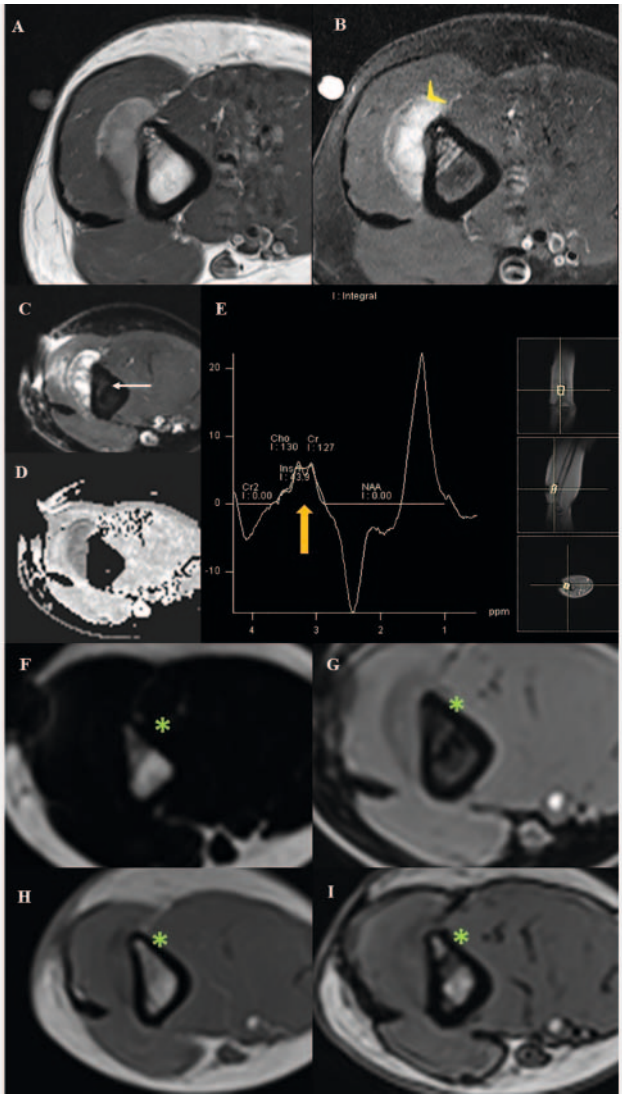

▶ **Fig. 5** Parosteal osteosarcoma of the distal humerus G2 in a 57-year-old female patient. On T1-weighted sequence **A**, the lesion is relatively hyperintense with respect to muscle. The low signal is also seen in the medullary canal, initially suspicious for bone marrow infiltration (arrow). **B** Heterogeneous high signal on T2-weighted sequence with a focal high signal of the underlying cortex and medulla (arrowhead). The lesion shows diffusion restriction on DWI **C** and ADC map **D** with no intramedullary restricted diffusion (white arrow). **E** Typical choline peak (hollow arrow) is seen on MR spectroscopy confirming the lesion's malignant nature. **F–i** Dixon QCSI sequences (asterisk) allow the exclusion of bone marrow infiltration.

▶ **Abb. 5** Parosteales Osteosarkom des distalen Humerus G2 bei einer 57-jährigen Patientin. **A** In der T1w erscheint die Läsion relativ hyperintens verglichen mit normalem Muskelsignal. Eine niedrige Signalintesität ist auch im Markraum sichtbar, wodurch sich initial der Verdacht auf eine Markrauminfiltration ergab (Pfeil). **B** Heterogen-angehobene Signalintensitäten des Tumors in der T2w mit fokalen Hyperintensitäten der darunter liegenden Kortikalis und des Markraumes (Pfeilspitze). Die Läsion zeigt eine Diffusionsrestriktion in der DWI **C** und ADC **D**, jedoch ohne Nachweis einer intramedullären Diffusionseinschränkung (weißer Pfeil). **E** Ein typischer Cholin-Peak (hohler Pfeil) in der MR-Spektroskopie bestätigt die Malignität der Läsion. **F** Mittels i-Dixon QCSI Sequenz (Stern) konnte eine Markrauminfiltration letztendlich ausgeschlossen werden.

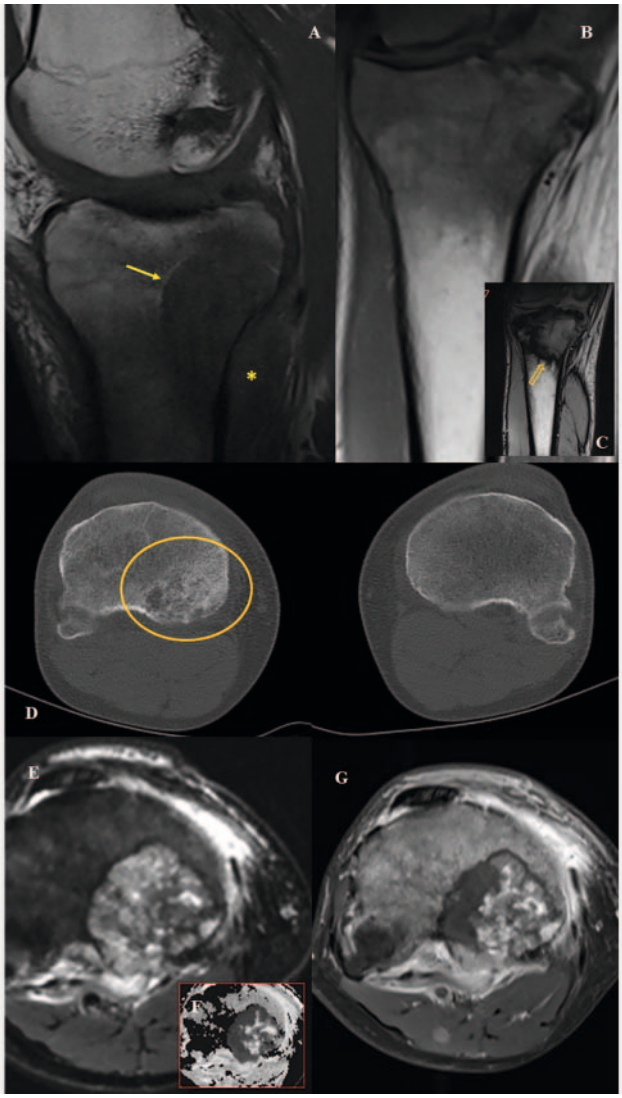

▶ **Fig. 6** Classic osteosarcoma of the proximal tibial metaphysis in a 47-year-old male patient. **A** Intraosseous (yellow asterisk) and extraosseous (white asterisk) extension of the tumor are seen on sagittal T1-weighted sequence. **B**, **C** Chemical shift imaging shows sharp delineation of the tumor and surrounding normal bone marrow with "India-ink artifact" on opposed phase (yellow arrow). **D** Corresponding axial CT of the lower extremities in the bone window shows osteodestructive lesion in the medial proximal tibial metaphysis (circle). Diffusion restriction of the osteosarcoma is seen on DWI and ADC maps **E**, **F**. **G** Post-gadolinium T1-weighted sequence shows heterogeneous enhancement of the tumor with hypovascularized tumor tissue centrally.

▶ **Abb. 6** Klassisches Osteosarkom der proximalen Tibiametaphyse bei einem 47-jährigen Patienten. **A** Intra- (gelber Stern) und extraossäre (weißer Stern) Ausdehnung des Tumors in der sagittalen T1w. **B**, **C** Die Chemical-Shift Bilder zeigen einen scharf begrenzten Tumor umgeben von unauffälligem Knochenmark, mit einem „India-ink" Artefakt in der Opposed-Phase (gelber Pfeil). **D** In der korrespondierenden axialen CT der unteren Extremität im Knochenfenster-Kernel zeigen sich Osteodestruktionen in der medialen proximalen Tibiametaphyse (Kreis). **E**, **F** Diffusionsrestriktionen des Osteosarkoms in der DWI und ADC Karte. **G** T1w nach Gadolinium-Applikation mit zentral hypovaskularisiertem Tumorgewebe bei heterogener Kontrastmittelaufnahme der übrigen Tumoranteile.

niques develop concurrently. Although cMRI is currently the state-of-the-art method for the characterization of bone and soft-tissue lesions, aMRI methods have become available and, in the future, have the potential to become the gold standard in sarcoma imaging. A shift from classic radiological image analysis toward radiomics – based on the extraction of radiomic features from data sets provided by CR, US, CT, and MRI – has the potential to positively impact clinical decision-making and the treatment management of patients with STS and BS.

Conflict of Interest

The authors declare that they have no conflict of interest.

References

[1] Biermann JS, Chow W, Reed DR et al. NCCN guidelines insights: bone cancer, version 2.2017. Journal of the National Comprehensive Cancer Network 2017; 15: 155–167

[2] Von Mehren M, Randall RL, Benjamin RS et al. Soft tissue sarcoma, version 2.2018, NCCN clinical practice guidelines in oncology. Journal of the National Comprehensive Cancer Network 2018; 16: 536–563

[3] Casali PG, Abecassis N, Bauer S et al. Soft tissue and visceral sarcomas: ESMO–EURACAN Clinical Practice Guidelines for diagnosis, treatment and follow-up. Annals of Oncology 2018; 29: iv51–iv67

[4] Crombé A, Marcellin PJ, Buy X et al. Soft-tissue sarcomas: assessment of MRI features correlating with histologic grade and patient outcome. Radiology 2019; 291: 710–721

[5] Asmar K, Saade C, Salman R et al. The value of diffusion weighted imaging and apparent diffusion coefficient in primary Osteogenic and Ewing sarcomas for the monitoring of response to treatment: Initial experience. European Journal of Radiology 2020; 124: 108855

[6] Patel DB, Matcuk GR Jr. Imaging of soft tissue sarcomas. Chin Clin Oncol 2018; 7: 35

[7] García-Figueiras R, Goh VJ, Padhani AR et al. CT perfusion in oncologic imaging: a useful tool? American Journal of Roentgenology 2013; 200: 8–19

[8] Drapé JL. Advances in magnetic resonance imaging of musculoskeletal tumours. Orthopaedics & Traumatology: Surgery & Research 2013; 99: S115–S123

[9] Siegel RL, Miller KD, Jemal A. Cancer statistics, 2016. CA: a cancer journal for clinicians 2016; 66: 7–30

[10] Jo VY, Fletcher CD. WHO classification of soft tissue tumours: an update based on the 2013 (4th) edition. Pathology 2014; 46: 95–104

[11] Robinson E, Bleakney RR, Ferguson PC et al. Multidisciplinary management of soft-tissue sarcoma. Radiographics 2008; 28: 2069–2086

[12] Levy AD, Manning MA, Al-Refaie WB et al. Soft-tissue sarcomas of the abdomen and pelvis: radiologic-pathologic features, Part 1—common sarcomas: from the radiologic pathology archives. Radiographics 2017; 37: 462–483

[13] Gruber L, Loizides A, Luger AK et al. Soft-tissue tumor contrast enhancement patterns: diagnostic value and comparison between ultrasound and MRI. American Journal of Roentgenology 2017; 208: 393–401

[14] Cohen J, Riishede I, Carlsen JF et al. Can Strain Elastography Predict Malignancy of Soft Tissue Tumors in a Tertiary Sarcoma Center? Diagnostics 2020; 10: 148

[15] James SL, Davies AM. Post-operative imaging of soft tissue sarcomas. Cancer Imaging 2008; 8: 8

[16] Yoon MA, Chee CG, Chung HW et al. Added value of diffusion-weighted imaging to conventional MRI for predicting fascial involvement of soft tissue sarcomas. European radiology 2019; 29: 1863–1873

[17] Ioannidis GS, Nikiforaki K, Karantanas A. Statistical and spatial correlation between diffusion and perfusion MR imaging parameters: A study on soft tissue sarcomas. Physica Medica 2019; 65: 59–66

[18] Sbaraglia M, Dei Tos AP. The pathology of soft tissue sarcomas. La radiologia medica 2019; 124: 266–281

[19] Corino VD, Montin E, Messina A et al. Radiomic analysis of soft tissues sarcomas can distinguish intermediate from high-grade lesions. Journal of Magnetic Resonance Imaging 2018; 47: 829–840

[20] Schneider N, Strauss DC, Smith MJ et al. The adequacy of core biopsy in the assessment of smooth muscle neoplasms of soft tissues. The American journal of surgical pathology 2017; 41: 923–931

[21] Barile A, Regis G, Masi R et al. Musculoskeletal tumours: preliminary experience with perfusion MRI. La radiologia medica 2007; 112: 550–561

[22] Bologna M, Montin E, Corino VDA et al. Stability assessment of first order statistics features computed on ADC maps in soft-tissue sarcoma. Annu Int Conf IEEE Eng Med Biol Soc 2017; 2017: 612–615

[23] Lee JH, Yoon YC, Seo SW et al. Soft tissue sarcoma: DWI and DCE-MRI parameters correlate with Ki-67 labeling index. European Radiology 2020; 30: 914–924

[24] Deshmukh S, Subhawong T, Carrino JA et al. Role of MR spectroscopy in musculoskeletal imaging. The Indian journal of radiology & imaging 2014; 24: 210

[25] Ferrari S, Bielack SS, Smeland S et al. EURO-BOSS: A European study on chemotherapy in bone-sarcoma patients aged over 40: Outcome in primary high-grade osteosarcoma. Tumori Journal 2018; 104: 30–36

[26] Douis H, Saifuddin A. The imaging of cartilaginous bone tumours. II. Chondrosarcoma. Skeletal radiology 2013; 42: 611–626

[27] Murphey MD, Senchak LT, Mambalam PK et al. From the radiologic pathology archives: Ewing sarcoma family of tumors: radiologic-pathologic correlation. Radiographics 2013; 33: 803–831

[28] Stacy GS, Mahal RS, Peabody TD. Staging of bone tumors: a review with illustrative examples. American Journal of Roentgenology 2006; 186: 967–976

[29] Mintz DN, Hwang S. Bone tumor imaging, then and now. HSS Journal® 2014; 10: 230–239

[30] Sá Neto JL, Simão MN, Crema MD et al. Diagnostic performance of magnetic resonance imaging in the assessment of periosteal reactions in bone sarcomas using conventional radiography as the reference. Radiologia brasileira 2017; 50: 176–181

[31] Aquerreta JD, San-Julián M, Benito A et al. Growth Plate Involvement in Malignant Bone Tumors: Relationship Between Imaging Methods and Histological Findings. InCañadell's Pediatric Bone Sarcomas. Cham: Springer; 2016: 129–137

[32] Tanaka K, Ozaki T. New TNM classification (AJCC eighth edition) of bone and soft tissue sarcomas: JCOG Bone and Soft Tissue Tumor Study Group. Japanese journal of clinical oncology 2019; 49: 103–107

[33] Gersing AS, Pfeiffer D, Kopp FK et al. Evaluation of MR-derived CT-like images and simulated radiographs compared to conventional radiography in patients with benign and malignant bone tumors. European radiology 2019; 29: 13–21

[34] Weber MA, Papakonstantinou O, Nikodinovska VV et al. Ewing's sarcoma and primary osseous lymphoma: spectrum of imaging appearances. InSeminars in musculoskeletal radiology. Thieme Medical Publishers 2019; 23: 036–057

[35] Gulia A, Puri A, Subi TS et al. Comparison of MRI and Histopathology with regard to Intramedullary Extent of Disease in Bone Sarcomas. Sarcoma 2019; 2019: 7385470

[36] Fayad LM, Jacobs MA, Wang X et al. Musculoskeletal tumors: how to use anatomic, functional, and metabolic MR techniques. Radiology 2012; 265: 340–356

[37] Uhl M, Saueressig U, van Buiren M et al. Osteosarcoma: preliminary results of in vivo assessment of tumor necrosis after chemotherapy with diffusion-and perfusion-weighted magnetic resonance imaging. Investigative radiology 2006; 41: 618–623

[38] Rao A, Sharma C, Parampalli R. Role of diffusion-weighted MRI in differentiating benign from malignant bone tumors. BJR Open 2019; 1: 20180048. doi:10.1259/bjro.20180048. PMID: 33178932; PMCID: PMC7592477

[39] Doganay S, Altinok T, Alkan A et al. The role of MRS in the differentiation of benign and malignant soft tissue and bone tumors. European journal of radiology 2011; 79: e33–e37

[40] Malek M, Kazemi MA, Saberi S et al. Diffusion-Weighted Imaging and Proton Magnetic Resonance Spectroscopy Findings in Osteosarcoma Versus Normal Muscle. Iranian Journal of Radiology 2017; 14

[41] Zhang Y, Yue B, Zhao X et al. Benign or Malignant Characterization of Soft-Tissue Tumors by Using Semiquantitative and Quantitative Parameters of Dynamic Contrast-Enhanced Magnetic Resonance Imaging. Canadian Association of Radiologists Journal 2020; 71: 92–99

[42] Rajiah P, Sundaram M, Subhas N. Dual-Energy CT in Musculoskeletal Imaging: What Is the Role Beyond Gout? American Journal of Roentgenology 2019; 213: 493–505

[43] Mallinson PI, Coupal TM, McLaughlin PD et al. Dual-energy CT for the musculoskeletal system. Radiology 2016; 281: 690–707

[44] Schiano C, Soricelli A, De Nigris F et al. New challenges in integrated diagnosis by imaging and osteo-immunology in bone lesions. Expert review of clinical immunology 2019; 15: 289–301

[45] Theruvath AJ, Siedek F, Muehe AM et al. Therapy Response Assessment of Pediatric Tumors with Whole-Body Diffusion-weighted MRI and FDG PET/MRI. Radiology 2020; 296: 143–151

[46] Baljer BC, Kolhe S, Chan CD et al. Advances in image enhancement for sarcoma surgery. Cancer letters 2020; 483: 1

[47] Vallières M, Freeman CR, Skamene SR et al. A radiomics model from joint FDG-PET and MRI texture features for the prediction of lung metastases in soft-tissue sarcomas of the extremities. Physics in Medicine & Biology 2015; 60: 5471

[48] Crombé A, Périer C, Kind M et al. T2-based MRI Delta-radiomics improve response prediction in soft-tissue sarcomas treated by neoadjuvant chemotherapy. Journal of Magnetic Resonance Imaging 2019; 50: 497–510

[49] Malinauskaite I, Hofmeister J, Burgermeister S et al. Radiomics and Machine Learning Differentiate Soft-Tissue Lipoma and Liposarcoma Better than Musculoskeletal Radiologists. Sarcoma 2020; 2020: 7163453

[50] Spraker MB, Wootton LS, Hippe DS et al. MRI radiomic features are independently associated with overall survival in soft tissue sarcoma. Advances in radiation oncology 2019; 4: 413–421

ERRATUM 23.11.2021

Erratum: Igrec J, Fuchsjäger MH. Imaging of Bone and Soft-Tissue Sarcomas. Fortschr Röntgenstr 2021; 193: 1171–1182

The institut of the authors was changed on 23.11.2021 to Division of General Radiological Diagnostics, Department of Radiology, Medical University of Graz, Austria.